

Constraining jet production scenarios by studies of Narrow-Line-Radio-Galaxies

Marek Sikora¹, Grażyna Stasińska², Dorota Koziel-Wierzbowska³, Greg M. Madejski⁴, and
Natalia V. Asari^{5,6}

ABSTRACT

We study a large sample of narrow-line radio galaxies (NLRGs) with extended radio structures. Using 1.4 GHz radio luminosities, $L_{1.4}$, narrow optical emission line luminosities, $L_{[\text{O III}]}$ and $L_{H\alpha}$, as well as black hole masses M_{BH} derived from stellar velocity dispersions measured from the optical spectra obtained with the Sloan Digital Sky Survey, we find that: (i) NLRGs cover about 4 decades of the Eddington ratio, $\lambda \equiv L_{bol}/L_{Edd} \propto L_{line}/M_{BH}$; (ii) $L_{1.4}/M_{BH}$ strongly correlates with λ ; (iii) radio-loudness, $\mathcal{R} \equiv L_{1.4}/L_{line}$, strongly anti-correlates with λ . A very broad range of the Eddington ratio indicates that the parent population of NLRGs includes both radio-loud quasars (RLQs) and broad-line radio galaxies (BLRGs). The correlations they obey and their high jet production efficiencies favor a jet production model which involves the so-called 'magnetically choked' accretion scenario. In this model, production of the jet is dominated by the Blandford-Znajek mechanism, and the magnetic fields in the vicinity of the central black hole are confined by the ram pressure of the accretion flow. Since large net magnetic flux accumulated in central regions of the accretion flow required by the model can take place only via geometrically thick accretion, we speculate that the massive, 'cold' accretion events associated with luminous emission-line AGN can be accompanied by an efficient jet production only if preceded by a hot, very sub-Eddington accretion phase.

Subject headings: radio galaxies: jets — production mechanisms

¹Nicolaus Copernicus Astronomical Center, Bartycka 18, 00-716 Warsaw, Poland; sikora@camk.edu.pl

²LUTH, Observatoire de Paris, CNRS, Université Paris Diderot, Place Jules Janssen 92190 Meudon, France

³Astronomical Observatory, Jagiellonian University, ul. Orla 171, 30-244 Kraków, Poland

⁴Kavli Institute for Particle Astrophysics and Cosmology, Stanford University, Stanford, CA 94305, USA

⁵Institute of Astronomy, University of Cambridge, Madingley Road, Cambridge, CB3 0HA, United Kingdom

⁶CAPES Foundation, Ministry of Education of Brazil, Caixa Postal 250, Brasilia - DF, 70040-020, Brazil

1. INTRODUCTION

It became clear already shortly after the discovery of first radio galaxies that their strong radio emission is associated with a presence of luminous optical emission lines (Bade & Minkowski 1954; Osterbrock 1977; Grandi & Osterbrock 1978). Such an association was later confirmed by finding a correlation of radio luminosities with narrow line luminosities in Fanaroff-Riley type II (FR II, Fanaroff & Riley 1974) radio sources (Baum & Heckman 1989; Saunders et al. 1989; Rawlings et al. 1989; Rawlings & Saunders 1991; Zirbel & Baum 1995; Willott et al. 1999; Buttiglione et al. 2010; Kozieł-Wierzbowska & Stasińska 2011: KS11). Using the narrow-line luminosity as a proxy for the cold accretion disk luminosity and the radio luminosity as a proxy of the jet power, Rawlings & Saunders (1991) found an approximate proportionality between these two quantities, with jet powers approaching and in some cases, even exceeding the bolometric luminosities of the accretion disks.

Studies of the correlation of the jet powers with properties of central engines using radio and optical luminosities became more thorough and robust once methods of the black hole mass estimations have been developed (see, e.g., Woo & Urry 2002 and refs. therein). This allowed a determination of the properties of radio-loud AGN as a function of their Eddington ratio, λ , defined as the ratio of the accretion bolometric luminosity to the Eddington luminosity. In particular, Kozieł-Wierzbowska & Stasińska (2011) using the black hole mass estimates from the stellar velocity dispersion (σ_*) – BH mass (M_{BH}) relation (Tremaine et al. 2002) found that FR II radio galaxies span about 4 decades of the Eddington ratio and that, when scaled by their black hole masses, their radio luminosities correlate with Eddington ratio, in similarity to the correlation of absolute radio luminosities vs. absolute narrow emission line luminosities. One might consider this similarity as resulting from the fact that distribution of the black hole masses of FR II sources is rather narrow, with majority of them within the range $10^8 - 10^9 M_\odot$. However, since the physics of the jet production is linked to the Eddington-scaled accretion rate rather than to its absolute value and powers of jets produced with the same efficiency scale with the black hole mass, the ‘primary correlation’ to be considered should be the one between the Eddington-scaled luminosities.

Such a correlation, however, contradicts the predictions of jet models which relate the strength of the central poloidal magnetic fields (those threading innermost portions of accretion disk and the black hole) with maximal pressure in the disk. According to the standard accretion disk theory, innermost portions of disks accreting at a rate corresponding to the Eddington ratio in the range $10^{-4} - 1$ are radiation pressure dominated. Since this pressure does not depend on the accretion rate, the powers of jets - believed to be initially dominated by Poynting flux - are not expected to depend on the accretion rate either. In consequence, such models predict maximal jet powers ~ 100 times smaller than those observed in RLQs

with extended radio structures (see, e.g., Ghosh & Abramowicz 1997).

The model which *can* account for the energetics of the most powerful jets and explain the observed radio - optical correlation is the one based on the so-called magnetically arrested/choked accretion flows (Narayan et al. 2003; Igumenshchev 2008; McKinney et al. 2012). In such a model, the amount of the net magnetic flux amassed in the central region is so large that innermost portions of accretion disks are dynamically affected by central magnetic fields. In this regime, the accretion onto a black hole proceeds via interchange instabilities (\equiv magnetic Rayleigh-Taylor instability: Stone & Gardiner 2007 and refs. therein) and magnetic flux threading the black hole is supported by the ram pressure of the accreting plasma.

In order to directly confront this model with observations, we expand the sample of radio galaxies studied by KS11 by including other types of radio morphologies, investigate the correlation of radio-loudness \mathcal{R} (radio-to-optical luminosity ratio) vs. λ , and investigate the dependence of source sizes on the Eddington ratio. The paper is organized as follows: in Section 2 we describe our sample selection and data reduction and analysis; in Section 3 we present results of our analysis of optical and radio based correlations; in Section 4 we investigate a consistency of these results with the jet production model which involves ‘magnetically-choked’ accretion scenario. Our main conclusions are listed in Section 5.

Throughout the paper we assume a Λ CDM cosmology with $H_0 = 71 \text{ km s}^{-1} \text{ Mpc}^{-1}$, $\Omega_m = 0.27$, and $\Omega_\Lambda = 0.73$.

2. THE DATA

2.1. The sample

To select our sample, we proceeded in a manner analogous to that described in KS11. Since we are primarily interested in radio galaxies with elongated structures, we started with Cambridge radio catalogs accessible by Vizier where such objects are well defined: 3C (Edge et al. 1959; Bennett 1962), 4C (Pilkington & Scott 1965; Gower et al. 1967), 5C (Pearson 1975; Pearson & Kus 1978; Benn et al. 1982; Benn & Kenderdine 1991; Benn 1995), 6C (Baldwin et al. 1985; Hales et al. 1988, 1990, 1991, 1993ab), 7C (Hales et al 2007), 8C (Rees 1990; Hales et al. 1995) and 9C (Waldram et al. 2003). We considered all the radio sources from these catalogs and cross-identified them in an automatic fashion with the sample of 926246 galaxies with optical spectra from the Sloan Digital Sky Survey (SDSS) DR7 main galaxy sample (Abazajian et al. 2009). Taking into account the sometimes large positional uncertainties in the Cambridge radio catalogs, we adopted a maximum distance between the

position given for the radio source and that given for the optical galaxy varying from 0.2 arcmin to 1 arcmin, depending on the catalog. We thus obtained a list of 2633 radio galaxies with available SDSS spectra. The final identification was done using the NVSS (Condon et al. 1998) and FIRST (Becker et al. 1995) radio maps, which have much better spatial resolution than the Cambridge catalogs, and have been obtained at the same frequency of 1.4 GHz. For all the pre-selected objects we constructed jpg images superimposing NVSS or FIRST contours on SDSS images in the r band. The images are centered on the galaxy which is supposed to correspond to the radio source. By visual inspection of all these images, we found that 307 cases were actually misidentifications (among which many of them corresponding indeed to a galaxy but for which the SDSS spectrum was that of another, nearby galaxy), and 14 corresponded to spiral galaxies whose radio emission is produced over the entire disk, most likely by star formation. For the remaining 2042 radio sources we carried out a morphological classification by eye resulting in the following subclasses:

- FR I type radio sources, considered as those where the maximum brightness of the lobes is closer to the center than to the extremity,
- FR II type, where the maximum brightness of the lobes is closer to the extremity,
- FR I/II type, where one lobe is of FR I type and the other of FR II type,
- double-double radio sources where two pairs of coaxial lobes are detected,
- X-shape radio sources with two pairs of lobes forming an X-shape structure,
- one-sided radio sources showing only one lobe,
- “elongated”, i.e. radio sources that do not appear point-like, but whose angular size does not allow us to classify them more accurately,
- radio sources, for which no morphological class could be assigned because of an atypical, irregular shape
- compact, unresolved radio sources.

This morphological classification, which is purely subjective, was carried out independently by two of the co-authors, DKW and GS. For about 15% of the objects we considered, our initial classifications diverged, although we agreed on our final classification. For further considerations in this paper, we restricted our sample to objects that clearly show the presence of radio structures associated with radio lobes and/or jets, i.e. FRII, FRI, FRII/FRI, double-double, X-shape and one-sided.

We excluded the radio sources whose parent galaxies have a redshift larger than 0.4, in order to insure that the $H\alpha$ emission line – which is crucial for our study – falls within the SDSS spectral range. We also excluded those radio sources where a broad component was clearly seen in the hydrogen emission lines. This allows us to make more accurate computations of narrow line luminosities as it avoids issues related to the decomposition of the narrow and the broad components. In addition, this limits our sample to objects which according to the Unified Scheme are observed at large inclination angles and by this step, we minimize viewing angle biases in our sample, in particular regarding source sizes. Finally, objects corresponding to galaxies where no emission lines were detected (after processing with the STARLIGHT code, Cid Fernandes et al. 2005, see below) were obviously removed from the sample, since all the considerations in this paper make use of emission line fluxes. After all these cuts, the entire sample on which this paper is based consists of 404 objects. They are listed in Table 1 (accessible only on-line), together with the properties that will be used.

There are some differences between our starting sample and the catalog of elongated radio sources published by Lin et al. (2010). The latter was assembled via cross correlation of the SDSS DR6 with NVSS and FIRST. Those radio surveys have the advantage of being more homogeneous and deeper than the Cambridge catalogs. Indeed, the limiting radio flux density at 1.4 GHz in Lin’s et al. sample is 3 mJy while that of the 3C catalog (when rescaled to 1.4 GHz) is 2 Jy, and those of the 4C-9C catalogs range between 400 mJy and 20 mJy (except for the 5C catalog which reaches 1.5 mJy but in very limited zones of the sky). One may wonder how many objects we are missing by using the Cambridge catalogs as a starting point rather than the NVSS one. It turns out that the number should not be very large, since our sample is limited to a redshift of 0.4, contains only objects with FRI, FRII and related morphologies which are the most luminous radio sources and, in addition, includes only objects with emission lines. All our objects have 1.4 GHz luminosities larger than 10^{24} W Hz $^{-1}$. In Lin’s et al. catalog, there are only 120 objects with radio luminosities smaller than that out of a total of 1040 objects. This implies that, in our sample, we miss at the very most 12% of objects on the low luminosity side. On the other hand, for some reason, our starting sample contains 112 objects that fulfil all the selection criteria of Lin et al. but do not appear in their catalog (such as, e.g. the well-known objects 3C198, 4C+00.56 which are bright in radio and have large angular sizes). Another difference between our approach and the one of Lin et al. is that, while they attempted to define an objective way to trace the galaxy population smoothly from FRI sources to FRII, (as opposed to a sharp and perhaps arbitrary distinction between type I versus type II), we adhered to more a classical morphological classification paying attention to other types than just FRI and FRII.

2.2. Data processing

The 1.4 GHz radio luminosities, $L_{1.4}$, were obtained for each source from the sum of 1.4 GHz fluxes of each of its components listed in the NVSS catalog, including the central, compact point source. The NVSS catalog was used here in order to avoid a flux loss from the extended and faint components missed in the FIRST catalog.

The determination of the angular sizes of the radio sources depended on the morphologies. For FRII radio sources, the angular sizes were defined as the distances between the hot spots or the most distant bright structures in opposite lobes. They were estimated from the FIRST maps, if available, or from the NVSS maps otherwise. The determination of the sizes of FRI radio sources is less straightforward, since lobes and plumes of the FRI radio galaxies fade away with the distance from the radio core. For each FRI source in our sample, we obtained the 3 rms contour using the FIRST map and we took for the source size the largest extent of this contour, measured along a straight line crossing the radio core (if present). This procedure works well with straight sources. In the case of bent sources, the size determined in that manner is an underestimate. For one-sided sources, we adopted a procedure similar to the one for FRI sources to determine the angular size of the only lobe. The linear (projected) sizes were then determined from the observed angular sizes using the redshift of the corresponding galaxy as obtained from the SDSS. To meaningfully compare the sizes of all the sources, we divided by two the sizes of all the two-sided radio-sources: the result is called the characteristic lobe-size in the remaining of this work.

The line luminosities of the galaxies associated with the radio sources are fundamental for our work. It is therefore important to determine them in the best possible way. For a removal of the stellar features from the observed optical spectrum, the best approach is to fit the observed continuum – excluding the spectral zones where emission lines are expected – with a composite stellar population obtained by spectral synthesis and subtract it from the entire observed spectrum. What remains is the pure emission line spectrum, whose intensities can then be measured. As in KS11, we have taken the [O III]5007, $H\alpha$ and $H\beta$ line fluxes from the STARLIGHT database¹, where they have been obtained precisely in this manner.

As argued in KS11, we consider $L_{H\alpha}$ to be a much better measure of the bolometric luminosity of the AGN than the commonly used $L_{[\text{O III}]}$, because it does not depend on the ionization state. This has also been shown by Netzer (2009). The plots presented below are, however, presented in pairs, with one plot using $L_{H\alpha}$ and the other using $L_{[\text{O III}]}$, for easy

¹see <http://www.starlight.ufsc.br>

comparison with works by other authors.

In only about 20% of objects in our sample are both the $H\alpha$ and $H\beta$ line fluxes measured with sufficient accuracy to allow a meaningful estimation of the extinction from their ratios. In the majority of those cases, the extinction A_V is smaller than 1 although in a couple of cases it reaches values of up to 4. Note that we find no correlation between A_V and the radio luminosity and the luminosity in the lines. There is then no other way than to ignore extinction in our work, if we want to work with a sample with significant size. Ignoring extinction will then simply add some dispersion to the properties derived from the comparison of optical and radio data, which is not really an issue in our work.

The black hole masses of the galaxies were estimated from the observed stellar velocity dispersion given by the SDSS, σ_* , using the relation by Tremaine et al. (2002):

$$\log M_{\text{BH}} = 8.13 + 4.02 \log(\sigma_*/200 \text{ km s}^{-1}). \quad (1)$$

In considerations involving black hole masses we disregard cases with $\sigma_* < 60 \text{ km s}^{-1}$ as well as cases where the signal-to-noise ratio of the SDSS spectrum at 4000 \AA is smaller than 10, to ensure that the estimate of M_{BH} is not significantly affected by observational errors.

3. RESULTS

3.1. Radio vs. optical luminosities

Figure 1 presents our sample of radio galaxies in the $L_{1.4} - L_{H\alpha}$ and $L_{1.4} - L_{[\text{O III}]}$ planes. Radio galaxies of FRI type are represented by filled red (grey in the printed edition) circles, FRII types by filled black circles, and the remaining types, i.e. FRI/II, double-double, X-shape and one-sided in open blue (grey in the printed edition) circles. As it is apparent from the figure, the radio luminosities strongly correlate with the narrow-line luminosities, with a Spearman rank correlation coefficient $r_S = 0.67$ for $H\alpha$ lines and $r_S = 0.62$ for $[\text{O III}]$ lines².

In the left panel of Figure 1 we also labelled the axes in units of P_j and L_{bol} , where P_j is the jet power and L_{bol} is the AGN bolometric luminosity. They are obtained by using the following conversion formulae:

²Rather than the widely used Pearson correlation coefficient to measure the strenghts of correlations, we prefer to consider the Spearman rank correlation coefficient which is appropriate for all the diagrams presented in this study. Indeed, the use of the Pearson correlation coefficient may lead to spurious interpretations of correlations in the case where both variables are scaled by a common factor (see e.g. Dunlap et al 1997, Barraclough 2007).

$$L_{bol} = 2.0 \times 10^3 L_{H\alpha} = 7.8 \times 10^{36} L_{H\alpha} [L_{\odot}] \text{erg s}^{-1}, \quad (2)$$

(Netzer 2009), and

$$P_j = 1.6 \times 10^{18} (f/3)^{3/2} L_{1.4} [\text{W Hz}^{-1}] \text{erg s}^{-1}, \quad (3)$$

the latter being taken from Willott et al. (1999) with the following modifications: (i) conversion from 151 MHz to 1.4 GHz assuming the spectral index $\alpha = 0.8$ ($L_{\nu} \propto \nu^{-\alpha}$); (ii) replacement of $P_j \propto L_{\nu}^{6/7}$ by $P_j \propto L_{\nu}$, the latter taken with a normalization factor giving equality of both at $L_{1.4} = 10^{26} \text{W Hz}^{-1}$. With this normalization the modified formula leads to overestimation of a jet power by a factor 1.4 for $L_{1.4} = 10^{27} \text{W Hz}^{-1}$ and underestimation by a similar factor for $L_{1.4} = 10^{25} \text{W Hz}^{-1}$. These differences are not substantial when compared with uncertainties of an original formula expressed via the parameter f , with its 1 – 20 range. The figure was made adopting $f=3$. One can see that even for low values of f the jet powers of many objects exceed their bolometric luminosities.

3.2. Radio luminosities vs. Eddington ratio

In Figure 2 we plot the radio vs. emission line luminosities normalized by the black hole mass. They correlate similarly strongly as their absolute values, with a Spearman rank correlation coefficient $r_S = 0.77$ and $r_S = 0.71$ for $H\alpha$ and $[\text{O III}]$ lines, respectively. Noting that L_{line}/M_{BH} provides the proxy for the Eddington ratio defined to be $\lambda \equiv L_{bol}/L_{Edd}$ and using the conversion formulae (2) and (3), one can see in the left panel of Figure 2 that NLRG cover about 4 decades of λ , from $\lambda \sim 10^{-4}$ up to $\lambda = 1$. The figure shows that our sample is dominated by objects with λ spanning the range of $10^{-4} - 10^{-2}$. These AGN are optically too weak to be considered as hidden quasars, but nonetheless, being emitters of strong and high excitation lines are expected to be powered like quasars by cold accretion disks and, if not obscured by torus, would appear to us as BLRGs (Urry & Padovani 1995). However, one should note that the division of AGN for RLQs and BLRGs does not have any physical grounds, they form continuous ‘Eddington ratio sequence’ with no signs of an accretion mode change (Sikora et al. 2007).³

The deficiency of AGN with $\lambda > 0.01$ in our sample confirms the earlier indications of rarity of very high accretion rate sources at low redshifts located in massive galaxies (see, e.g., Kauffmann et al. 2008), while the presence of several FRI RGs at $\lambda > 0.01$ is consistent

³Historically the AGN division to RLQs and BLRGs was related to the stellar vs. fuzzy optical appearance of host galaxies, presently it is usually related to the specific value of the AGN absolute optical magnitude, e.g. $M_B = -23.0$ as in the Véron-Cetty & Véron catalogs (1993).

with a direct finding by Heywood et al. (2007) that radio morphologies of type FRI – which are usually associated with low luminosity RGs – do happen in quasars as well.

3.3. Radio-loudness vs. Eddington ratio

In Figure 3 we plot the dependence of $L_{1.4}/L_{line}$ on L_{line}/M_{BH} , where $L_{1.4}/L_{line}$ can be considered to be the proxy of the radio-loudness defined as the radio-to-optical flux ratio. Our results show a significant negative correlation of radio-loudness with the Eddington ratio, with a Spearman rank correlation coefficient $r_S = -0.54$ and $r_S = -0.63$ when using the $H\alpha$ and $[O\ III]$ lines, respectively. Such an anti-correlation was discovered previously by Ho (2002) for radio quiet AGN and by Sikora et al. (2007) for radio-loud AGN, however, the statistics of their studies was too poor to claim its presence in the sample when limited only to strong-emission-line objects.

In the left panel of Figure 3 we have also indicated the values of P_j/L_{bol} and λ on the axes. We can see that most objects with $\lambda < 0.01$ have jet powers exceeding bolometric luminosity of their AGN, those with lowest λ 's even by a factor larger than $10 (f/3)^{3/2}$ (see Eq. 3).

3.4. Sizes

Figure 4 shows the sizes of the radio lobes as a function of the Eddington ratio obtained using $H\alpha$ (left panel) and $[O\ III]$ (right panel). To our knowledge, this is the first time that such a diagram is shown. There is only a weak correlation, with a Spearman rank correlation coefficient $r_S = 0.34$ and $r_S = 0.27$ when using the $H\alpha$ and $[O\ III]$ lines, respectively. This suggests that the expansion of radio sources is not accompanied by monotonic, long term changes of the accretion rate, and that product of expansion velocity multiplied by the source life-time does not depend on the Eddington ratio. Furthermore, the fact that the source sizes show no dependence with morphological type suggests that radio morphologies do not form any evolutionary sequence. However one cannot exclude “switches” between different morphologies caused by modulations of the jet power and the jet direction.

4. DISCUSSION

Amongst all AGN, the most spectacular from the observational standpoint, yet most challenging theoretically – are probably those associated with extended, luminous radio

structures. They appear to us as BLRGs and RLQs if oriented with respect to our line of sight such that their nuclei are not obscured by dusty tori, and as NLRG otherwise. Their radio and optical luminosities imply an efficient energy transport from nuclei to radio-lobes via narrow relativistic jets at a rate very often exceeding the bolometric luminosities of their host nuclei (Rawlings & Saunders 1991; Ghisellini et al. 2010; Fernandes et al. 2011; Punsly 2011; and Section 3 in this paper).

As it was demonstrated by Tchekhovskoy et al. (2011) and McKinney et al. (2012), such powerful jets can be produced in the scenario which involves magnetically arrested/choked accretion flows. Such an accretion mode can well take place in the innermost portions of a disk, when the amount of the net magnetic flux, Φ , amassed in the central region is larger than the maximal flux which can be imparted on that region around the black hole by the ram pressure of accreting plasma,

$$\Phi_{BH} = \phi_{BH} R_g (\dot{M})^{1/2}, \quad (4)$$

where \dot{M} is the accretion rate, $R_g = GM_{BH}/c^2$, and ϕ_{BH} is the dimensionless factor called by Tchekhovskoy et al. (2011) the “dimensionless magnetic flux.” The value of ϕ_{BH} depends on the details of the model and according to the numerical simulations by McKinney et al. (2012) is typically on the order of 50.⁴ Jets powered by rotating black holes threaded by such magnetic flux appear to gain kinetic luminosities (Blandford & Znajek 1977; Tchekhovskoy et al. 2010)

$$P_j \simeq 4.0 \times 10^{-4} \frac{1}{c} \Phi_{BH}^2 \Omega_{BH}^2 f(\Omega_{BH}) \sim 10 (\phi_{BH}/50)^2 x_a^2 f(x_a) \dot{M} c^2, \quad (5)$$

where

$$x_a \equiv R_g \Omega_{BH} / c = [2(1 + \sqrt{1 - a^2})]^{-1} a \quad (6)$$

$$f(x_a) \simeq 1 + 1.4x_a^2 - 9.2x_a^4 \quad (7)$$

and $a \equiv J_{BH}/J_{BH,max} = cJ_{BH}/GM_{BH}^2$ is the dimensionless angular momentum of a BH, commonly named ‘spin’. For maximal black hole spins, $a \sim 1$ ($\rightarrow x_a \sim 1/2$),

$$P_{j,max} \simeq 1.9(\phi_{BH}/50)^2 \dot{M} c^2 = 19(\phi_{BH}/50)^2 L_{bol}/(\epsilon/0.1). \quad (8)$$

where $\epsilon = L_{bol}/(\dot{M} c^2)$ is the radiation efficiency of an accretion disk. The jet power may also contain a contribution from the accretion flow. However, as it was shown by McKinney et al. (2012) this contribution is never dominant and therefore will be ignored in our further

⁴Note that dimensionless magnetic flux defined by McKinney et al. (2012) and denoted by Υ_{BH} is lower by a factor 5, and is found to be typically of the order of 10.

discussion. As it can be verified using Eqs. (5) and (8) and Figures 1 and 2, the model predicts domination of jet powers over AGN bolometric luminosities even for moderate spins.

As the next step, we will investigate whether – and how – such a model can explain the anti-correlation of radio-loudness with Eddington ratio shown in Fig. 3. We have

$$\mathcal{R} = L_{1.4}/L_{line} \propto P_j/L_{bol} = P_j/(\epsilon \dot{M} c^2) = \eta_j/\epsilon \quad (9)$$

where $\eta_j \equiv P_j/\dot{M} c^2$ is often referred to as the jet production efficiency. Hence the negative correlation of \mathcal{R} with λ may potentially arise from the respective dependencies of η_j and/or ϵ on λ . According to Eq. (5), the dependence of η_j on λ can eventually result from the dependence of the spin on λ . However that would require a negative correlation of spins with λ , which is the opposite of what one might expect by noting that the black holes are span up more efficiently for larger rather than smaller accretion rates. Hence we are left with the option that the disk accretion efficiency decreases with the decrease of the Eddington ratio, i.e. that ϵ correlates with λ .

The correlation can be explained if assuming that all cold accretion episodes start with a similar total net magnetic flux Φ , which is sufficiently large to exceed Φ_{BH} for any accretion rate (see Eq. 4). In such a case, the dynamical dominance of magnetic field over the accreting plasma extends up to $R_m \gg R_{in}$, where R_{in} is the inner edge of a standard accretion disk not affected by magnetic fields, and R_m , sometimes referred to as the magnetospheric radius, is the size of the region within which the magnetic flux Φ is enclosed. Since below that radius the accretion proceeds via interchange instabilities, no significant optical-UV radiation is expected to be produced within this region. Hence, being ‘truncated’ at R_m , the accretion disk is expected to have radiation efficiency $\epsilon \sim R_g/R_m$. Noting that for a given black hole mass $R_m/R_g \propto (\Phi)^{4/3} \dot{m}^{-2/3}$ (Narayan et al. 2003) where $\dot{m} \equiv \dot{M} c^2/L_{EDD} = \lambda/\epsilon$, one can find that $\epsilon \propto \lambda^{2/5}$ and therefore that

$$\mathcal{R} \propto \eta_j/\epsilon \propto \lambda^{-2/5}. \quad (10)$$

Some dispersion is expected to be imposed on this relation by distributions of black hole masses and magnetic fluxes (unless $\Phi \propto M_{BH}^{3/2}$).

The large ratios R_m/R_g for AGN with low values of λ are consistent with detailed observations of some individual BLRGs which strongly suggest existence of the truncation radius in their accretion disks (Eracleous et al. 2000; Grandi & Palumbo 2007; Sambruna et al. 2009; Tazaki et al. 2010; Cowperthwaite & Reynolds 2012). In those papers, the disk truncation radii inferred from observations were interpreted as an effect of obscuration of the central region by Thomson thick corona, or as a transition to the advection dominated accretion flows. Since it predicts large truncation radii as determined by R_m , the model can

explain the cases of objects with $P_j/L_{bol} > 10$ (see Punsly 2011 and refs. therein) without the necessity to postulate the jet production efficiency significantly greater than unity.⁵

The scenario presented above needs to be verified by demonstrating how such large net magnetic flux can be assembled in the central regions of AGN. This problem was raised by Lubov et al. (1994), who showed that it is possible only if the magnetic Prandtl number is $\leq H/R$, where H is the height of the disk at a distance R from the black hole center. Since the Prandtl number predicted in fluids with isotropic turbulence is expected to be on the order of unity (Parker 1979), the above condition is rather difficult to satisfy in cold, geometrically thin disks (Livio et al. 1999; Cuo 2011). This problem can be alleviated, if one considers a possibility of an accumulation of a large magnetic flux in the central regions of AGN at the onset, or even prior to the period of the cold accretion phase. Such an accumulation could occur by dragging magnetic fields by geometrically thick, advection dominated accretion flows, such as those predicted for super-Eddington accretion rates (Jaroszyński et al. 1980; Beloborodov 1998; Abramowicz 2005) and also for very sub-Eddington accretion rates (Ichimaru 1977; Rees et al. 1982; Narayan & Yi 1994). Since our studies of source sizes do not indicate any evolutionary trends of expansion of sources with decreasing Eddington ratio (Fig. 4), the second option seems to be favored. This is also supported by probabilistic arguments. For a given frequency of the cold accretion events, which in turn are very likely to be triggered by mergers of giant ellipticals with less massive, cold gas - rich galaxies (see Ramos Almeida et al. 2012 and refs. therein), the fraction of those events accompanied by production of powerful jets is predicted to correspond to a reasonably significant fraction ($\sim 3 - 10\%$) of giant ellipticals to be in radio-active states (Sadler et al. 1989; Donoso et al. 2009; van Velzen et al. 2012). These ellipticals are most likely powered by the Bondi accretion of hot interstellar gas (Burns 1990; Hardcastle et al. 2007; Tasse et al. 2008; Dunn et al. 2010; Werner et al. 2012). For typical intensities of interstellar magnetic fields in such galaxies, $\sim 10\mu\text{G}$, and their coherence scales, ~ 100 parsecs (Moss & Shukurov 1996; Mathews & Brighenti 2003 and refs. therein), the accumulation magnetic fluxes in the central regions of such objects needed to exceed Φ_{BH} for any accretion rate can occur within a small fraction of the Hubble time.

⁵Formally η_j can exceed unity, which simply would mean that the rate of extraction of the black hole's rotational energy is larger than the rate of the energy inflow (Tchekovskoy et al. (2011)). However as most recent simulations of McKinney et al. (2012) indicate, it is rather difficult to achieve such a solution.

5. CONCLUSIONS

Main results of our studies of radio and spectroscopic optical properties of NLRGs at $z < 0.4$ can be summarized as follows:

- Radio luminosities are found to correlate strongly with narrow line luminosities. When converted to the jet powers and AGN bolometric luminosities, they indicate that the jet kinetic energy often exceeds the radiative output of accretion flows;
- NLRGs cover about 4 decades of the Eddington ratio, λ , with most of them having $\lambda < 0.01$. This indicates that their parent population is dominated by BLRGs. Together with RLQ they form a continuous Eddington ratio sequence;
- The 'radio-loudness', $\mathcal{R} = L_{1.4}/L_{line}$, shows a strong negative correlation with λ . This would imply that the jet production efficiency is the largest at lowest values of λ , provided disk radiation efficiency is independent on λ .
- The lack of any signatures of correlation or anti-correlation of radio source sizes with Eddington ratio indicates the lack of any significant monotonic migration of objects (to lower or larger Eddington ratios);
- A promising scenario which can explain energetics of jets in powerful radio sources and observed radio vs. optical luminosity correlations is the one involving the magnetically arrested/choked accretion flows. Such flows may support sufficiently large magnetic fluxes to power jets with $P_j \gtrsim L_{bol}$, while a truncation of accretion disks by a 'poloidal magnetosphere' can relax requirements of having $\eta_j \gtrsim 1$.
- Our results suggest a connection of the cold accretion phase following a lower accretion rate, hot accretion phase taking place in extragalactic radio sources. Such a two-phase scenario can overcome the difficulty of accumulating large magnetic fluxes by geometrically thin accretion disks. Without such a pre-phase, the cold accretion events would not be accompanied by production of powerful jets.

MS and GM are grateful to R. Blandford and J. McKinney for many stimulating discussions regarding magnetically-choked accretion scenarios. We acknowledge financial support by the Polish NCN grant DEC-2011/01/B/ST9/04845, by NASA Fermi grant no. NNX11AO39G, and by a Herschel Research Support Agreement (grant administered by NASA JPL) no. RSA 1433865. GS and DKW acknowledge financial support from the European Associated Laboratory "Astrophysics Poland-France". NVA has been supported by CAPES (proc. no. 6382-10-0)

REFERENCES

- Abazajian, K. N., Adelman-McCarthy, J. K., Agüeros, M. A., et al. 2009, *ApJS*, 182, 543
- Abramowicz, M. A. 2005, *Growing Black Holes: Accretion in a Cosmological Context*, 257
- Baade, W., & Minkowski, R. 1954, *ApJ*, 119, 215
- Baldwin, J. E., Boysen, R. C., Hales, S. E. G., et al. 1985, *MNRAS*, 217, 717
- Barracough, K., 2007, *Scaling regression equations: solution or problem?*, Working paper, Vanderbilt University.
- Baum, S., & Heckman, T.M. 1989, *ApJ*, 336, 702
- Becker, R. H., White, R. L., & Helfand, D. J. 1995, *ApJ*, 450, 559
- Beloborodov, A. M. 1998, *MNRAS*, 297, 739
- Benn, C. R., Gruett, G., Vigotti, M., & Wall, J. V. 1982, *MNRAS*, 200, 747
- Benn, C. R. 1995, *MNRAS*, 272, 699
- Benn, C. R., & Kenderdine, S. 1991, *MNRAS*, 251, 253
- Bennett, A. S. 1962, *MmRAS*, 68, 163
- Blandford, R. D., & Znajek, R. L. 1977, *MNRAS*, 179, 433
- Burns, J.O. 1990, *AJ*, 99, 14
- Buttiglione, S., Capetti, A., Celotti, A., et al. 2010, *A&A*, 509, A6
- Cid Fernandes, R., Schoenell, W., Gomes, J. M., et al. 2009, *Revista Mexicana de Astronomia y Astrofisica Conference Series*, 35, 127
- Condon, J. J., Cotton, W. D., Greisen, E. W., et al. 1998, *AJ*, 115, 1693
- Cowperthwaite, P.S., & Reynolds, C.S. 2012, *ApJ*, 752, L21
- Cuo, X. 2011, *ApJ*, 737, 94
- Donoso, E., Best, P. N., & Kauffmann, G. 2009, *MNRAS*, 392, 617
- Dunlap, W. P., Dietz, J., Cortina, J. M. , 1997, *Journal of General Psychology*, 124, 182
- Dunn, R.J.H., Allen, S.W., Taylor, G.B., et al. 2010, *MNRAS*, 404, 180

- Edge, D. O., Shakeshaft, J. R., McAdam, W. B., Baldwin, J. E., & Archer, S. 1959, *MmRAS*, 68, 37
- Eracleous, M., Sambruna, R., & Mushotzky, R.F. 2000, *ApJ*, 537, 654
- Fanaroff B. L., & Riley J. M., 1974, *MNRAS*, 167, 31P
- Fernandes, C. A. C., Jarvis, M. J., Rawlings, S., et al. 2011, *MNRAS*, 411, 1909
- Ghisellini, G., Della Ceca, R., Volonteri, M., et al. 2010, *MNRAS*, 405, 387
- Ghosh, P., & Abramowicz, M. A. 1997, *MNRAS*, 292, 887
- Gower, J. F. R., Scott, P. F., & Wills, D. 1967, *MmRAS*, 71, 49
- Grandi, S.A., & Osterbrock, D.E. 1978, *ApJ*, 220, 783
- Grandi, P. & Palumbo, G.G.C. 2007, *ApJ*, 659, 235
- Hales, S. E. G., Baldwin, J. E., & Warner, P. J. 1988, *MNRAS*, 234, 919
- Hales, S. E. G., Baldwin, J. E., & Warner, P. J. 1993, *MNRAS*, 263, 25
- Hales, S. E. G., Masson, C. R., Warner, P. J., & Baldwin, J. E. 1990, *MNRAS*, 246, 256
- Hales, S. E. G., Masson, C. R., Warner, P. J., Baldwin, J. E., & Green, D. A. 1993, *MNRAS*, 262, 1057
- Hales, S. E. G., Mayer, C. J., Warner, P. J., & Baldwin, J. E. 1991, *MNRAS*, 251, 46
- Hales, S. E. G., Riley, J. M., Waldram, E. M., Warner, P. J., & Baldwin, J. E. 2007, *MNRAS*, 382, 1639
- Hales, S. E. G., Waldram, E. M., Rees, N., & Warner, P. J. 1995, *MNRAS*, 274, 447
- Hardcastle, M.J., Evans, D.A., & Croston, J.H. 2007, *MNRAS*, 376, 1849
- Heywood, I., Blundell, K.M., & Rawlings, S. 2007, *MNRAS*, 381, 1093
- Ho, L. C. 2002, *ApJ*, 564, 120
- Ichimaru, S. 1977, *ApJ*, 214, 840
- Igumenshchev, I.V. 2008, *ApJ*, 677, 317
- Jaroszynski, M., Abramowicz, M. A., & Paczynski, B. 1980, *Acta Astron.*, 30, 1

- Kauffmann, G., Heckman, T. M., & Best, P. N. 2008, MNRAS, 384, 953
- Kozieł-Wierzbowska, D. & Stasińska, G. 2011, MNRAS, 415, 1013
- Lin, Y.-T., Shen, Y., Strauss, M. A., Richards, G. T., & Lunnan, R. 2010, ApJ, 723, 1119
- Livio, M., Ogilvie, G.I., & Pringle, J.E. 1999, ApJ, 512, 100
- Lubov, S.H., Papaloizou, J.C.B., & Pringle, J.E. 1994, MNRAS, 267, 235
- Mathews, W. G., & Brighenti, F. 2003, ARA&A, 41, 191
- McKinney, J. C., Tchekhovskoy, A., & Blandford, R. D. 2012, MNRAS, 423, 3083
- Moss, D., & Shukurov, A. 1996, MNRAS, 279, 229
- Narayan, R., Igumenshchev, I.V., & Abramowicz, M.A. 2003, PASJ, 55, L69
- Narayan, R., & Yi, I. 1994, ApJ, 428, L13
- Netzer H., 2009, MNRAS, 399, 1907
- Osterbrock, D.E. 1977, ApJ, 215, 733
- Parker, E. N. 1979, Oxford, Clarendon Press; New York, Oxford University Press, 1979
- Pearson, T. J. 1975, MNRAS, 171, 475
- Pearson, T. J., & Kus, A. J. 1978, MNRAS, 182, 273
- Pilkington, J. D. H., & Scott, P. F. 1965, MmRAS, 69, 183
- Punsly, B. 2011, ApJ, 728, L17
- Ramos Almeida, C., Bessiere, P. S., Tadhunter, C. N., et al. 2012, MNRAS, 419, 687
- Rawlings, S., & Saunders, R. 1991, Nature, 349, 138
- Rawlings, S., Saunders, R., Eales, S. A., & Mackay, C. D. 1989, MNRAS, 240, 701
- Rees, N. 1990, MNRAS, 244, 233
- Rees, M. J., Begelman, M. C., Blandford, R. D., & Phinney, E. S. 1982, Nature, 295, 17
- Sadler, E. M., Jenkins, C. R., & Kotanyi, C. G. 1989, MNRAS, 240, 591
- Sambruna, R.M., Reeves, J.N., Braito, V., et al. 2009, ApJ, 700, 1473

- Saunders, R., Baldwin, J. E., Rawlings, S., Warner, P. J., & Miller, L. 1989, MNRAS, 238, 777
- Sikora, M., Stawarz, L., & Lasota, J.-P. 2007, ApJ, 658, 815
- Stone, J.M., & Gardiner, T. 2007, ApJ, 671, 1726
- Tasse, C., Best, P.N., Röttgering, H., & Le Borgne, D. 2008, A&A, 490, 893
- Tazaki, F., Ueda, Y., Ishino, Y., et al. 2010, ApJ, 721, 1340
- Tchekhovskoy, A., Narayan, R., & McKinney, J. C. 2010, ApJ, 711, 50
- Tchekhovskoy, A., Narayan, R., & McKinney, J. C. 2011, MNRAS, 418, L79
- Tremaine, S., Gebhardt, K., Bender, R., et al. 2002, ApJ, 574, 740
- Urry, C.M., & Padovani, P. 1995, PASP, 107, 803
- van Velzen, S., Falcke, H., Schellart, P., Nierstenhöfer, N., & Kampert, K.-H. 2012, A&A, 544, A18
- Veron-Cetty, M.-P., & Veron, P. 1993, ESO Scientific Report, 13, 1
- Waldram, E. M., Pooley, G. G., Grainge, K. J. B., et al. 2003, MNRAS, 342, 915
- Werner, N., Allen, S.W., & Simionescu, A. 2012, MNRAS, in press (arXiv:1205.1563)
- Willott, C.J., Rawlings, S., Blundell, K.M., & Lacy, M. 1999, MNRAS, 309, 1017
- Woo, J.-H., & Urry, C.M. 2002, ApJ, 579, 530
- Zirbel, E.L., & Baum, S.A. 1995, ApJ, 448, 521

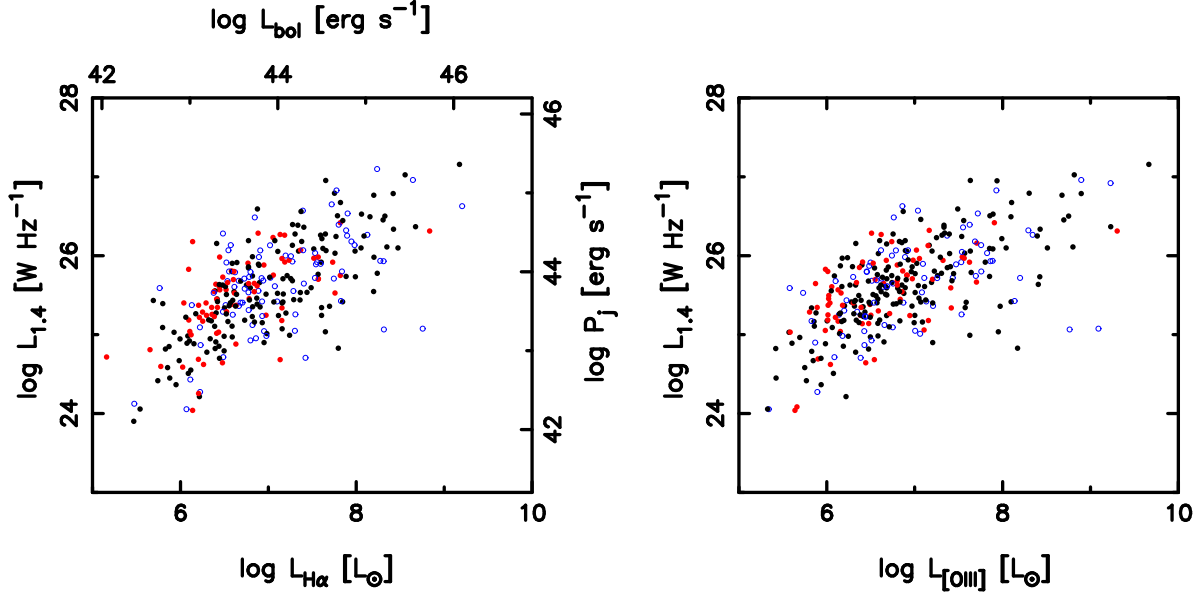


Fig. 1.— The radio luminosities $L_{1.4}$ as a function of the optical line luminosities $L_{\text{H}\alpha}$ (left panel) and $L_{[\text{O III}]}$ (right panel). FRI types are represented by filled red circles (grey in the printed edition), FRII types by filled black circles, and the remaining types, i.e. FRI/II, double-double, X-shape and one-sided in open blue circles (grey in the printed edition). In the left panel, the values of the bolometric luminosity and of the radio luminosity P_j in ergs s^{-1} calculated for $f = 3$ are also indicated.

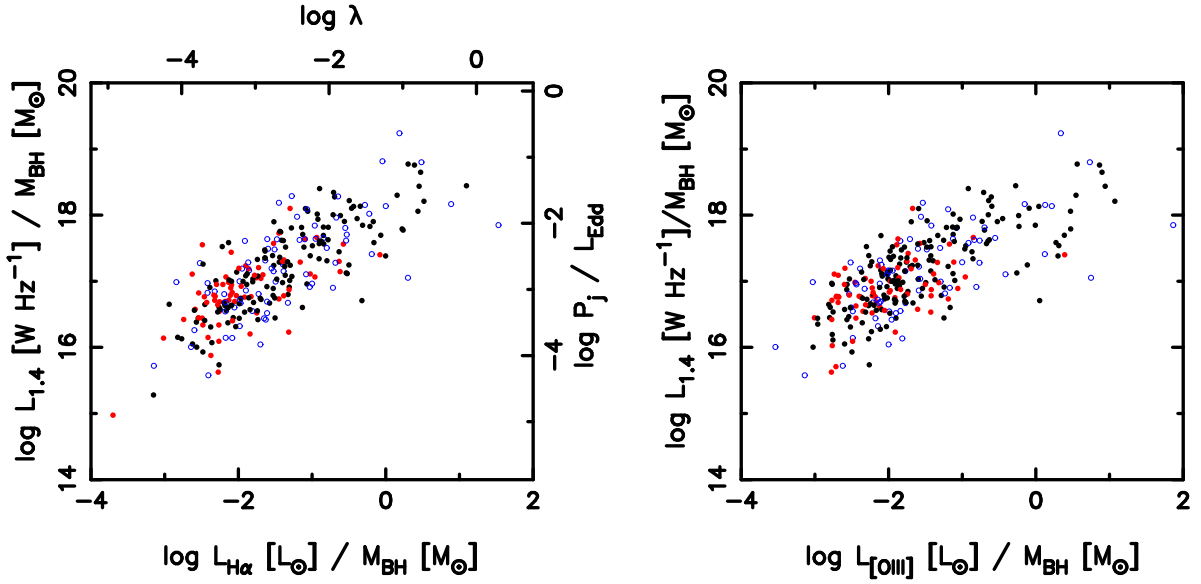


Fig. 2.— The radio luminosities normalized by the black hole masses as a function of optical emission line luminosities (left panel: $L_{\text{H}\alpha}$, right panel: $L_{[\text{OIII}]}$) normalized by the black hole masses. The symbols have the same meaning as in Fig. 1. In the left panel are also indicated the values of the parameters $\log \lambda$ and $\log P_j / L_{\text{Edd}}$ for $f = 3$.

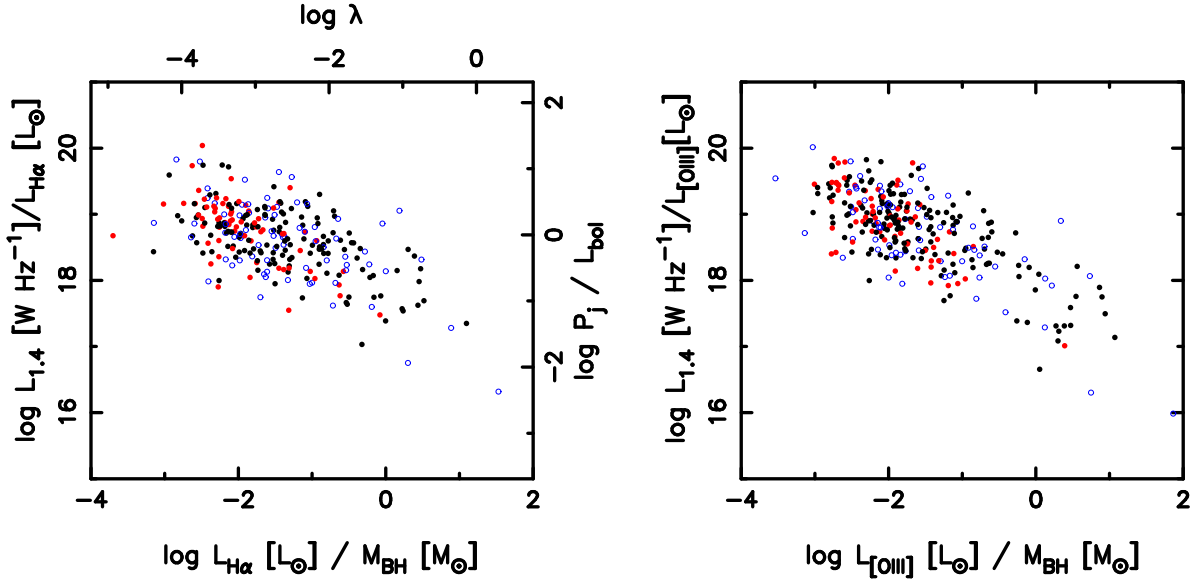


Fig. 3.— $L_{1.4}/L_{\text{H}\alpha}$ as a function of $L_{\text{H}\alpha}/M_{\text{BH}}$ (left panel) and $L_{1.4}/L_{[\text{OIII}]}$ as a function of $L_{[\text{OIII}]} / M_{\text{BH}}$ (right panel). The symbols have the same meaning as in Fig. 1. In the left panel are also indicated the values of the parameters $\log \lambda$ and $\log P_j / L_{\text{bol}}$ for $f = 3$.

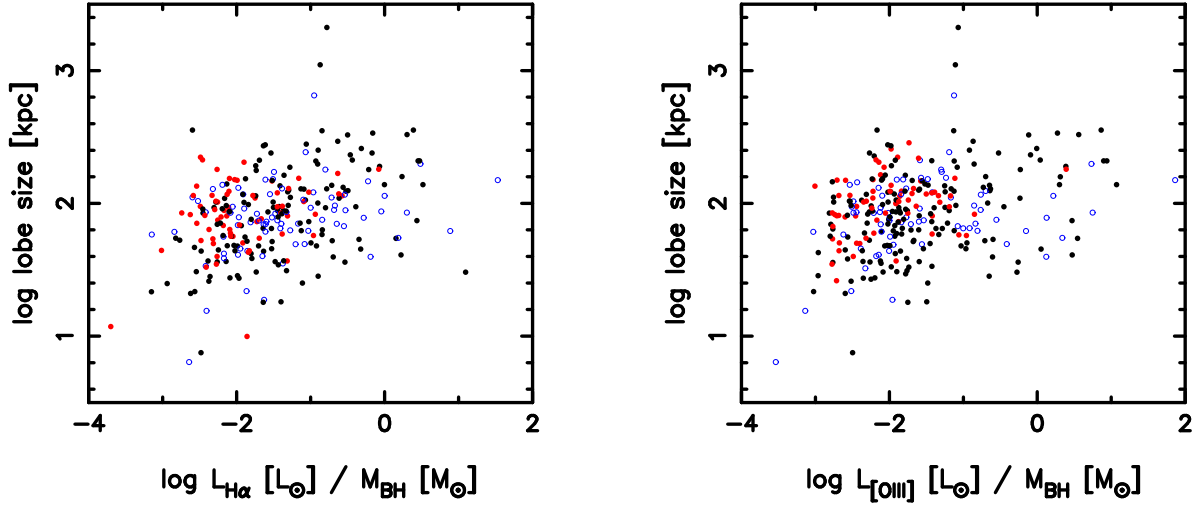


Fig. 4.— The projected sizes of the radio lobes as a function of the Eddington ratio, as measured using $\text{H}\alpha$ (left panel) and $[\text{O III}]$ (right panel). The symbols have the same meaning as in Fig. 1.

Table 1. Radio and optical properties of the sample of radio galaxies¹

SDSS ID	Cambridge Cat. ID	Redshift	Radio Type	$\log L_{1.4}$ (W Hz ⁻¹)	$\log L_{\text{H}\alpha}$ (L_{\odot})	$\log L_{[\text{O III}]}$ (L_{\odot})	$\log M_{\text{BH}}$ (M_{\odot})	Ang. size (arcsec)	Lobe size (kpc)
0273.51957.633	4C +00.37	0.0968	FRI	25.65	6.839	6.644	8.87	170.64	151.02
0312.51689.471	4C +00.56	0.0524	FR II	25.34	7.605	7.572	8.74	255.62	128.83
0349.51699.169	6C B165818.4+630042	0.1063	FR II	25.45	6.417	6.579	7.83	139.2	135.45
0366.52017.349	6C B171944.8+591634	0.2212	FR II	25.59	7.486	6.889	8.29	52	92.72
0367.51997.294	4C +54.36	0.1852	X-shaped	26.00	7.195	6.740	8.16	78	121.12
0385.51877.485	4C -00.83	0.1848	FRI/II	26.28	6.482	0.000	9.01	67.2	104.18
0400.51820.424	4C +00.05	0.0793	FRI/II	25.37	6.127	0.000	8.55	45	33.71
0432.51884.345	7C B073404.1+402639	0.3905	FR II	25.59	0.000	6.806	8.66	32	84.73
0436.51883.010	6C B075738.1+435851	0.2554	FR II	25.66	6.899	6.740	8.42	26	51.63
0439.51877.044	6C B080758.9+434635	0.1432	X-shaped	25.55	6.886	0.000	8.26	28	35.21
0439.51877.436	7C B080310.1+452158	0.2439	FRI	25.06	0.000	7.105	8.17	30.46	57.97
0439.51877.637	7C B081405.1+450809	0.1422	FR II	25.43	5.690	6.322	8.17	35	43.76
0442.51882.241	6C B081421.2+500530	0.2804	FRI/II	25.93	7.272	0.000	8.67	33	70.12
0442.51882.258	6C B081520.7+495611	0.0952	One-sided	24.87	6.227	6.426	8.20	45.03	78.53
0448.51900.335	6C B084421.9+571115	0.1937	FR II	26.08	7.515	7.887	7.98	144	231.62
0449.51900.323	7C B084921.8+544832	0.1133	FRI	25.57	6.519	0.000	8.38	9.78	9.95
0450.51908.330	4C +56.17	0.1409	FR II	26.05	7.107	6.912	8.04	170	208.59
0451.51908.541	7C B091959.0+571901	0.2846	FRI	25.24	6.973	6.500	8.72	51.55	109.78
0484.51907.497	6C B090602.0+585910	0.2698	X-shaped	26.25	7.894	7.367	8.45	32.90	67.43
0486.51910.456	7C B093527.5+622203	0.2298	FR II	25.41	0.000	6.277	8.65	58	105.59
0487.51943.188	6C B095114.5+625546	0.2286	FRI	25.62	6.871	0.000	8.92	31.17	56.48
0488.51914.191	6C B101400.2+634442	0.1839	X-shaped	25.72	7.021	7.431	8.43	42	64.85
0490.51929.096	7C B105806.3+654923	0.1926	FR II	25.15	6.928	6.992	8.24	76.2	122.08

¹Table 1 is published in its entirety in the electronic edition of ApJ. A portion is shown here for guidance regarding its form and content.